Available online at www.sciencedirect.com
ScienceDirect
Ceramics International 37 (2011) 2755–2761
CERAMICS INTERNATIONAL
www.elsevier.com/locate/ceramint

Spark plasma sintering to restrict sintering reactions and enhance properties of hydroxyapatite–mullite biocomposites

Ashutosh Kumar Dubey, Geet Sitesh, Shekhar Nath, Bikramjit Basu *

Laboratory for Biomaterials, Materials Science and Engineering, Indian Institute of Technology, Kanpur 208016, Uttar Pradesh, India

Received 26 March 2011; accepted 18 April 2011
Available online 27 April 2011

Abstract

Herein, we demonstrate how spark plasma sintering (SPS) can be useful in restricting the sintering reactions and faster densification in Hydroxyapatite–Mullite system, which otherwise shows extensive sintering reactions during conventional pressureless sintering, as reported in a recent study [Nath et al. J. Am. Ceram. Soc. 93 (2010) 1639–1649]. The microstructure of SPSed Hydroxyapatite (HAp)-20 wt% mullite composites was characterized by submicron sized HAp and equiaxed mullite grains. Another important result has been the achievement of higher hardness of 7 GPa, which is much higher than pressureless sintered composites. The cell culture study including cellular viability using MTT analysis establishes good cytocompatibility of SPSed composites.

Keywords: Hydroxyapatite; Mullite; Spark Plasma Sintering; Cell adhesion

1. Introduction

In the field of medical orthopedics, HAp [$Ca_{10}(PO_4)_6(OH)_2$] has been widely investigated for application in orthopedic/dental implant due to their quasi-identical composition to the mineral component of bone and teeth [1]. Despite this similarity, HAp has very limited applications in orthopedic implants due to its poor mechanical properties. To address such problems, HAp has been reinforced with second phase additions like ZrO_2 [2,3], Al_2O_3 [4,5], etc. to improve the mechanical properties, without considerably affecting its biocompatibility. In recent research [6–11], the idea of using mullite ($3Al_2O_3{\cdot}2SiO_2$) has been presented and a series of studies were carried out to understand sintering- microstructure-property correlation in HAp–mullite system, followed by detailed *in vitro* and *in vivo* biocompatibility study on optimal composites. The studies revealed that HAp-20 wt% mullite (after sintering it became bi-calcium phosphate (BCP)-mullite composites) composition showed better combination of physical and biological properties. A high compressive strength of close to 300 MPa was measured with BCP-20 wt% mullite composites along with a moderate improvement in fracture toughness (~1.5 MPa $m^{1/2}$ measured by SEVNB technique). The *in vitro* cytocompatibility results confirmed that BCP-mullite composite supported favorable cell proliferation of osteoblast like cells and mouse fibroblast cells. More importantly, the short term implantation in rabbits revealed good *in vivo* biocompatibility property of this composite. Therefore, HAp with 20 wt% mullite composition was chosen for spark plasma sintering experiments.

During pressureless sintering of HAp-20 wt% mullite composition, extensive sintering reactions led to the formation of β-TCP (major phase), gehlenite, Al_2O_3, CaO and HAp (minor phase). These were confirmed by XRD and TEM analysis, as reported elsewhere [7]. The development of multiphase microstructure led to lower hardness (3.5 GPa) and was certainly related to longer holding time at high sintering temperature. In recent times, spark plasma sintering (SPS) has been used as a rapid densification route to densify various materials [12–15]. Due to the applied electric field, the diffusion rate increases and therefore, powder can be densified at much lower temperature with shorter holding time (only few minutes). HAp–ZrO_2 [16] and HAp–Al_2O_3 [17,18] containing composites have already been prepared by SPS technique and the results showed improved properties compared to their pressureless sintered composites. However, no study is reported

* Corresponding author.
E-mail address: bikram@iitk.ac.in (B. Basu).

0272-8842/$36.00
doi:10.1016/j.ceramint.2011.04.032

to assess the efficacy of SPS to restrict sintering reactions in HAp-based highly reactive system, like HAp–mullite.

In the above backdrop, it is interesting to investigate whether SPS can be used to densify HAp-20 wt% mullite (HAp-20 M) composition at lower sintering temperature with shorter holding time and also to tailor sintering conditions in order to restrict sintering reactions. In addition, the physical and biocompatibility properties of these SPSed composites are also evaluated.

2. Experimental details

2.1. Starting powders

For the present work, HAp was synthesized by the widely reported chemical route [19]. Calcium oxide (CaO) and phosphoric acid (H_3PO_4) were used as the precursor materials and HAp precipitated following the reaction [1].

$$10CaO + 6H_3(PO)_4 = Ca_{10}(PO_4)_6(OH)_2 + 8H_2O \quad (1)$$

For the preparation of HAp, CaO was dispersed (14.6 g/l) in water medium and due to their poor solubility, H_3PO_4 (0.17 M) was added drop wise in to the solution. The reaction was completed at 80 °C after 3–4 h and the pH was adjusted to 10 for HAp precipitation. After 24 h, the precipitate was collected and dried followed by calcination at 800 °C. Sharp HAp peaks were confirmed from the XRD results. Therefore, 20 wt% mullite (KCM Corporation, Japan) was mixed with HAp and ball milled for 16 h in acetone medium. After milling, the slurry was dried and then crushed into fine powder in an agate mortar.

2.2. Sintering

Appropriate amount of dried powder mixtures were placed in a graphite die having 15.4 mm internal diameter and proper dressing with graphite sheet was done inside the die to avoid contamination. This entire die assembly was transferred carefully into the spark plasma sintering chamber (SPS Syntex INC, model: SPS-515S, Kanagawa, Japan) and placed in between the graphite electrodes. These electrodes transfer pressure and current to the die assembly. Vacuum of 50 m torr and pressure of 30 MPa were maintained throughout the experiment. DC current of 0.5–1.5 kA and DC voltage of 5–10 V were applied during the SPS experiments. All the powder mixtures were sintered in temperature range of 1000 °C to 1200 °C with a soaking time of 5 min. The heating rate of 50 °C/min and cooling rate of 25 °C/min were maintained. The cooling rate was kept low to reduce the thermal stresses. The temperature during entire SPS processing was monitored by focusing an optical pyrometer on the graphite die. The final thickness of the spark plasma sintered composite was around 2–3 mm. The removal of the graphite sheet around the sample was ensured before further characterization.

2.3. Characterization of sintered composites

The density of the sintered sample was measured by Archimedes's principle. The theoretical densities of composites were calculated using rule of mixture. XRD analysis was carried out using Cu-Kα radiation (λ = 1.5405 Å, scan rate 1°/min) to identify different phases in starting powders as well as sintered materials. Microstructure was observed on chemically etched surface as well as on fracture surface of the composites by scanning electron microscopy (SEM). The bulk hardness was determined from Vickers micro indentation experiments. The indents were taken on smoothly polished (0.25 μm surface finish) pellets with 0.1 kg load. Fracture toughness (K_{IC}, indentation toughness) calculations were based on the crack length measurements of the radial crack pattern produced by Vicker's (H_{V2}) indentations, according to the formula of Anstis et al. [20].

2.4. Cell culture experiments

L929 mouse fibroblast cells, obtained from CCMB Hyderabad, India, were used for cell-culture experiments. The cells were cultured in Dulbecco's modified Eagles medium (DMEM) supplemented with 10% fetal bovine serum (FBS) and 1% penicillin/streptomycin solution. The culture plate was incubated in an incubator (5% CO_2 and 90% humidity) at 37 °C temperature. After two days of incubation, the sub-confluent monolayer of cells was harvested from the culture plate using 0.5% trypsin and 0.2% EDTA solution. The same process was repeated one more time before the cells were seeded on the materials surfaces.

2.5. Cellular adhesion tests

As stated in Section 2.4, L929 cells were maintained in DMEM culture medium supplemented with 10% FBS and 1% penicillin/streptomycin solution. Sintered composites (1100, 1150, and 1200 °C) and control glass disc (gelatin coated) were used in the cell adhesion experiments. All the samples were sterilized in an autoclave (121 °C, 15 lb pressure) for 15 min and exposed with ultraviolet light for 30 min. Following this, samples were soaked in 70% ethanol for 30 min. The samples were then washed twice with phosphate buffer saline (PBS) and subsequently, the cells were seeded on the samples in 4 well culture plates. The culture plates were placed in CO_2 incubator. After the stipulated time period (24 h), the samples were washed twice with PBS to remove the culture medium completely and then fixed with 1.5% glutaraldehyde in PBS. The cells, adhered on the materials surface, were then dehydrated using a series of ethanol solutions (30, 50, 70, 95 and 100%) for 10 min twice and then further dried using critical point drier (CPD: Quramtech UK). The dried samples were sputter coated with gold and observed under SEM to understand the cell adhesion behavior. As the surface roughness plays an important role in cell-material interaction. Prior to cell culture, roughness measurement of polished samples revealed R_a values of less than 0.2 μm for all the samples.

2.6. MTT assay

MTT is a rapid colorimetric method. Mitochondrial enzymes of metabolically active cells react with Tetrazolium

salt (3(4,5-dimethylthiazol-2-yl)-2,5-diphenyl tetrazolium bromide, MTT) and form purple color formazan crystals. The cells viability was investigated on composites of HAp-20 M and pure HAp. The fibroblast cells (L929) were seeded on sterilized samples and the culture plate was incubated for 48 h in CO_2 incubator. Thereafter, the samples were washed twice with PBS and 200 μl DMEM (without phenol red and serum) was added. In the next step, 20 μl MTT (5 mg/ml in DMEM) was added in each well and plate was incubated for 6 h. The culture plate was viewed in the phase contrast microscope (Nikon- Eclipse80i, Japan) to check for the formation of purple color crystals. After the incubation, MTT solution was removed and crystals were dissolved by adding 200 μl of DMSO. The samples were removed from wells and optical density of the solutions were measured at 490 nm using ELISA automated microplate reader (Bio-Tek, model ELx800). In the present study, the MTT assay was carried out on composites (sintered at 1100 °C and 1200 °C) and pure HAp (sintered at 1050 °C). The cell viability in terms of metabolically active cells, was calculated using the following formula [21]:

$$\% \text{ viability} = \left(\frac{\text{mean absorbance of sample}}{\text{mean absorbance of control}}\right) \times 100.$$

3. Results and discussion

3.1. Sintered phases and microstructure

Fig. 1 presents X-ray diffraction (XRD) patterns of HAp-20 M, sintered at different temperatures. XRD of pure HAp and pure mullite SPSed at 1050 and 1500 °C, respectively, are also included for comparison. It can be noted that HAp was stable upto 1150 °C. A critical observation is that HAp began to dissociate to β-TCP, when sintered at 1200 °C. The dehydroxylation reaction can be written as:

$$2Ca_5(PO_4)_3(OH) \rightarrow 3Ca_3(PO_4)_2 + CaO + H_2O \quad (2)$$

Also, the presence of CaO and mullite peaks after sintering at 1200 °C indicated that unlike the case of pressureless sintering, mullite and CaO did not react. This could be due to the very short (5 min) soaking time and lower sintering temperature. The absence of other reaction products such as gehlenite and alumina, unlike pressureless sintering, also support the fact that mullite and CaO did not react in case of SPS.

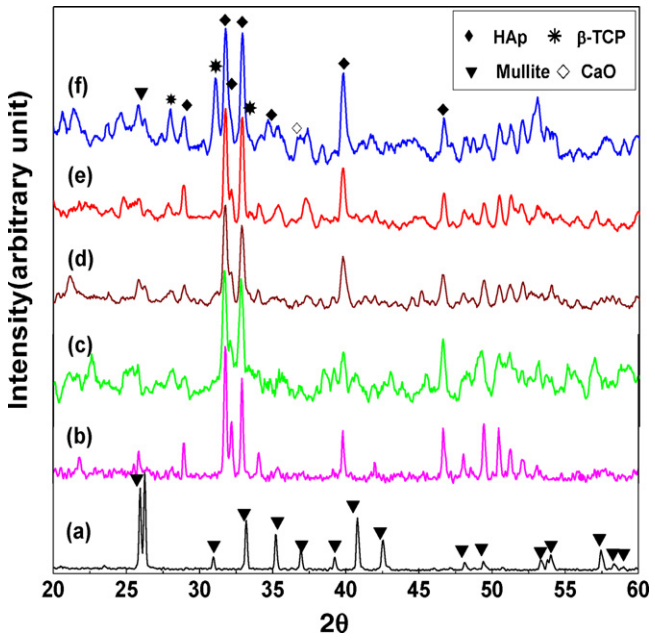

Fig. 1. XRD spectra from (a) pure mullite, SPSed at 1500 °C, (b) Pure HAp at 1050 °C and HAp – 20 M SPSed at varying temperatures- (c) 1050 °C (d) 1100 °C (e) 1150 °C (f) 1200 °C. All were SPSed for 5 min with 30 MPa pressure.

In the present set of experimental conditions, the main characteristic of the HAp–mullite system was that there was no chemical reaction with the mullite. In case of HAp–ZrO_2 composites [16] sintered by SPS technique, formation of $CaZrO_3$ is reported and HAp also dissociated to TCP at around 1075 °C for 5 min with 4.5–17.3 MPa pressure. However, Shen et al. [22] and Li and Gao [23] showed that HAp–ZrO_2 SPSed composites did not dissociate and did not produce any reaction products, when sintered at 1150 °C with 50 MPa pressure for 5 min and 3 min, respectively. From the present experimental conditions (30 MPa pressure) and combining the literature results it can be said that high sintering pressure plays an important role to restrict the HAp dissociation reaction (reaction [2]) upto 1150 °C.

The surface topography and fracture surface of HAp-20 M composites, SPSed at 1100 °C are presented in Fig. 2. Fig. 2a shows chemically etched surface microstructure. The HAp grains were comparatively bigger (600–800 nm) than the mullite grains (150–200 nm). Overall, the microstructure was much finer in SPSed composite, compared to that observed under pressureless sintering route. Mullite second phase was mainly present at the grain boundary region and at the triple junction of HAp grains. Also, mullite grains were well dispersed in the HAp matrix and most of the mullite grains are in contact with at least one HAp grain. Here, an important observation is that mullite grains are equiaxed, in contrast to the elongated grains (needle shaped) in the case of pressureless sintered composites. This kind of faceted shape of mullite also confirms the absence of liquid phase during sintering [6]. The fracture surface presented in Fig. 2(b) shows that the fracture mechanism was mainly transgranular type, which was typical in case of brittle materials. However, in some localized regions, fracture through grain pull out was also visible.

3.2. Densification, hardness and fracture toughness

The sinter density data for HAp-20 M, processed at various temperatures for 5 min are shown in Fig. 3. In all cases, the theoretical density was calculated in reference to the composition of the starting powder mixture as there were almost no or very little reactions between HA and mullite. Looking at Fig. 3, it is clear that a modest increase in SPS temperature from 1050 to 1100 °C increased the density from less than 95% ρ_{th} to close to 99% ρ_{th}. However, a further increase in SPS temperature did not have much influence, as

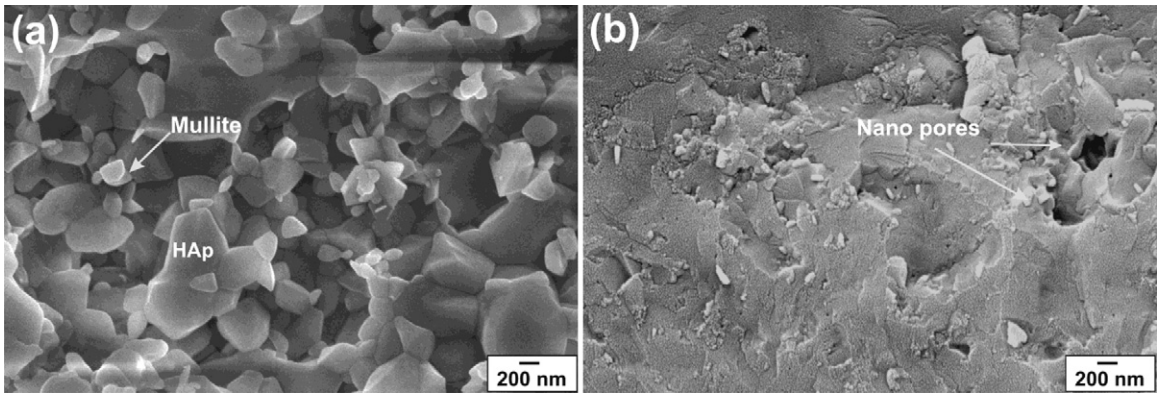

Fig. 2. (a) Surface topography of chemically etched and (b) fracture surface of HAp-20 M composites SPSed at 1100 °C for 5 min with 30 MPa pressure.

density varied insignificantly with an increase in SPS temperature to 1150 °C. The optimal densification was achieved for the HAp-20 M composite at 1100 °C. The density decrease at 1200 °C could be attributed to the formation of lower density phase (β-TCP). Comparing these density values with that of the pressureless sintered samples, it can be clearly understood the usefulness of SPS technique over pressureless technique. It should be noted that HAp-20 M was densified at 1350 °C in pressureless sintering. It can be suggested that densification in SPS occurred due to the combination of solid state sintering and plastic flow [24] mechanism. Though HAp and mullite both are non-conductive materials, the faster atomic mobility and higher diffusion rate in presence of applied electric field increased faster densification.

Fig. 3 also shows the Vickers hardness values of HAp-20 M samples, sintered at different temperatures. The hardness variation followed similar trend as that of the densification curve. The hardness increased from 3.2 GPa to 7.1 GPa, as SPS temperature increased from 1050 to 1100 °C. Also, no significant variation in hardness was measured for the samples, sintered above 1100 °C. It is to be noted here that using the same composition, a maximum hardness of 3.5 GPa was obtained using pressureless sintering technique. Comparing with the densification curve, it can be said that both densification and hardness curves followed similar trends with varying SPS temperatures. Therefore, densification had a direct correlation with the hardness values. It is clear that spark plasma sintering played a significant role to obtain high hardness in the composite. In case of pressureless sintering, the hardness was decreased due to the formation of softer sintered phases, like CaO and gehlenite [6]. Considering high hardness value of pure mullite (Fig. 3) in the present SPSed samples, the hardness values did not follow the rule of mixture. This could be due to the presence of nanopores as observed in SEM fracture surface observation (Fig. 2b). Also, the sintering temperature of pure mullite in SPS is much higher than 1200 °C. Therefore, the mullite–mullite particle contacts may act as weak interface, culminating lower hardness than that of calculated values obtained by rule of mixture. Fig. 4 shows a well developed indent shape with stable crack growth from the four corners.

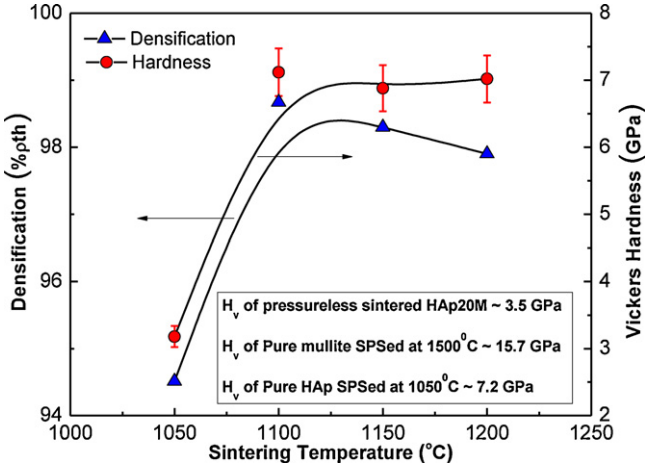

Fig. 3. Sintered density and Vickers' hardness as a function of sintering temperature for HAp-20 M using SPS technique. The theoretical density is calculated base on starting composition of the composites. The hardness values were obtained at 0.1 kg load and were calculated from average diagonals of indent.

Fracture toughness of different HAp-20 M samples have been evaluated and plotted in Fig. 5. The sample, sintered at 1100 °C showed highest fracture toughness of ~1.5 MPam$^{0.5}$. The increase in toughness at 1200 °C in comparison to that at

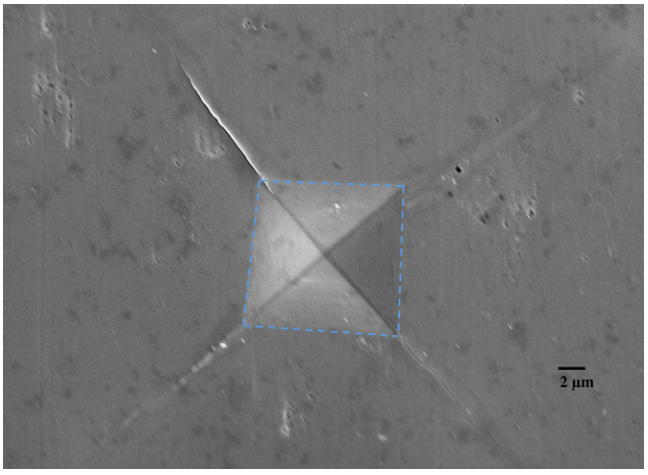

Fig. 4. Vickers indentation (0.1 kg load) taken on HAp-20 wt% mullite sample, SPSed at 1100 °C.

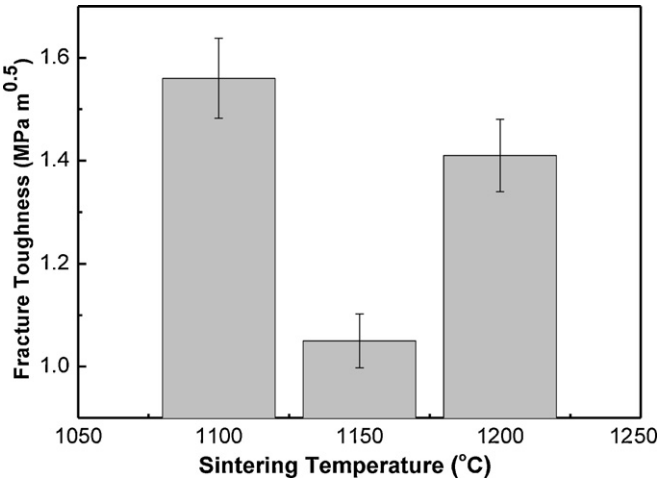

Fig. 5. Fracture toughness (indentation toughness) of HAp-20 wt% mullite composite sintered at different temperature by SPS.

1150 °C may be attributed to the formation of a softer CaO at 1200 °C. The fracture toughness was improved in comparison to that of pure HAp (∼0.6 MPam$^{0.5}$). This was probably due to the presence of mullite grains, which deflected the cracks through the weak mullite–mullite grain boundary (Fig. 2b).

3.3. In vitro biocompatibility

For the evaluation of cell adhesion, HAp-20 M, SPSed at 1100 °C was selected and the representative SEM images illustrating the cell adhesion after 24 h of culture are presented in Fig. 6. It is clear from Fig. 6 that fibroblast cells can adhere and proliferate on the developed composites. The cell adhesion and morphology on the developed composites were similar to the control sample. The cells adhered on the surface with their extended lamellipodia, an indication of cell migration. From a closure view [Fig. 6(c)], it was observed that apart from extended lamellipodia, the cells were attached with the neighboring cells through their multiple filopodia. The filopodia branching on the materials surface will give rise to better anchorage. In summary, the observed SEM images clearly revealed the cell adhesion, proliferation and cell to cell contacts on the surface of the developed composite material.

MTT is a well known colorimetric assay for quantitative determination of metabolically active cells on the materials surfaces. The measured optical density, as recorded with ELISA plate reader is directly proportional to the number of viable cells adhered on the samples surface.

Fig. 7 plots the MTT assays results using L929 mouse fibroblasts cells for the developed composite materials with reference to the negative control (Pure HAp). The MTT assay results showed that in case of HAp-20 M sample sintered at 1100 °C and 1200 °C, the number of metabolically active cells was more than that of pure HAp. The results showed that about 150% cell viability with respect to that of pure HAp sample. This enhanced cell viability was due to the presence of Si ion in case of HAp–mullite composites. It is already reported that Si doped BCP ceramics showed enhanced cell proliferation [25]. Kim et al. [26] found that silica (SiO_2) directly stimulate the

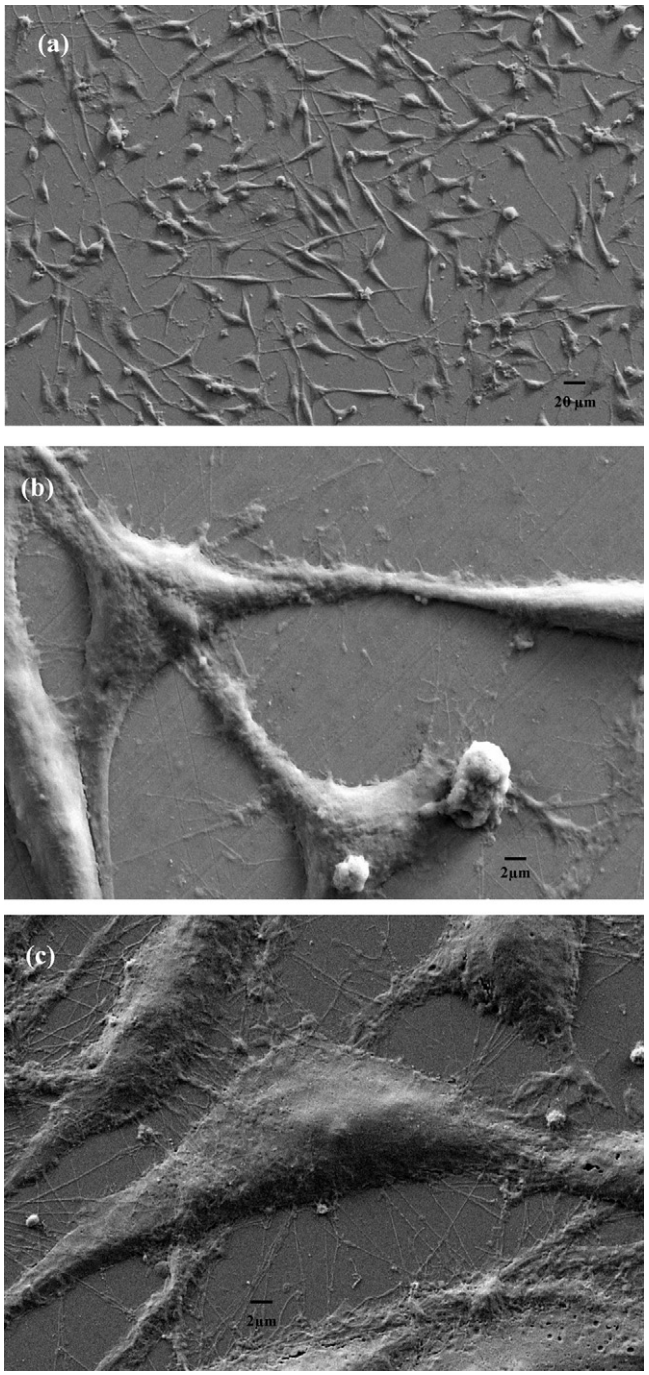

Fig. 6. SEM images of L29 cells adhered on (a), (b) HAp-20 wt% mullite (sintered at 1100 °C) and (c) on negative control sample. Results were obtained after 24 h of culture.

proliferation of rat fibroblast cell. Absher and Mortara [27] showed that silica enhanced proliferation rate of some human lung fibroblast cells. Mullite is a solid solution of Al_2O_3 and SiO_2. Therefore, in the present case the high proliferation rate of L929 cells on HAp–mullite composite surface showed similar stimulation effect.

It needs to be state here that, in case of pressureless sintering, HA partially dissociated into TCP, which form biphasic calcium phosphate (BCP) matrix in HA-20% mullite composite. In contrast, no detectable dissociation from HA to TCP

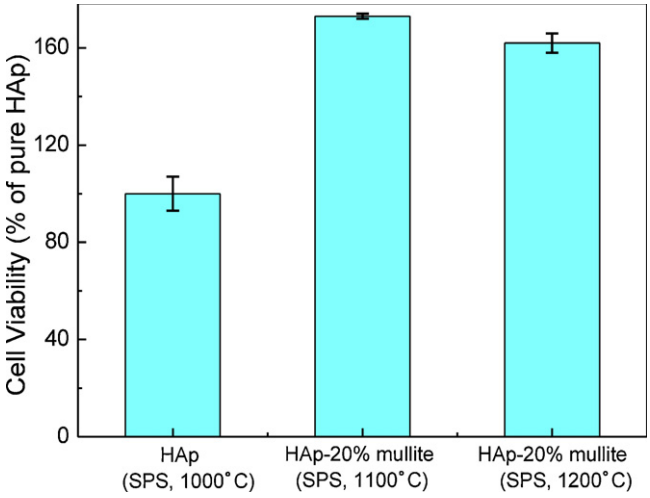

Fig. 7. MTT result shows cell viability of HAp-20 wt% mullite SPSed at 1100 °C and 1200 °C. The results were compared with pure HAp SPSed at 1000 °C.

occurred, when SPSed at below 1200 °C and therefore, the cell culture tested samples essentially have HA matrix. While comparing with the cell viability of pressureless sintered composites with BCP matrix, the results of the present study clearly indicates that even HA matrix based mullite composites can support good cell adhesion and viability. Also, the presence of mullite in bulk biocomposites did not cause any toxicity, as higher OD is recorded after MTT assay with the SPSed composite samples, than pure HA.

4. Conclusions

(a) The results of the spark plasma sintering experiments revealed that fully dense (∼98%ρ_{th}) HAp-20 wt% mullite composite can be obtained after spark plasma sintering at 1100 °C for 5 min, whereas the same composite composition with equivalent density required pressureless sintering at 1350 °C for 2 h.

(b) XRD analysis showed that unlike the pressureless sintering, the sintering reactions could be completely restricted in SPS sintered samples, as the dissociation of HAp and no reaction product could be recorded when SPSed at up to 1150 °C within the detection limit of XRD. The average grain size of the mullite phase was around 200 nm, however, HAp matrix is little courser (600–800 nm).

(c) The hardness measurements revealed that a high hardness of more than 7 GPa was achievable after spark plasma sintering at 1100 °C for 5 min, whereas a maximum hardness of 3.5 GPa was measured in pressureless sintering route.

(d) The combination of cell culture experiments and MTT analysis using L929 fibroblast cells provided clear evidences that the SPSed HAP-20 wt% Mullite composite supported cell adhesion and higher cell viability compared to pure HAp. The observation of cellular bridges, i.e. cell–cell interaction as well as flattening of the cells indicated good cytocompatibility property of the developed composite.

Acknowledgements

The authors thank DST, and DBT, Government of India for financial assistance to procure SPS set up and cell culture facility at IIT Kanpur, respectively.

References

[1] B.D. Ratner, A.S. Hoffman, F.J. Schoen, J.E. Lemons, Biomaterials Science: An Introduction to Materials in Medicine, Elsevier Academic Press, London, 2004.
[2] S. Gautier, E. Champion, D.B. Assollant, Processing, microstructure and toughness of Al_2O_3 platelet-reinforced hydroxyapatite, J. Eur. Ceram. Soc. 17 (1997) 1361–1369.
[3] J. Li, B. Fartash, L. Hermansson, Hydroxyapatite–alumina composites and bone-bonding, Biomaterials 16 (1995) 417–422.
[4] R.R. Rao, T.S. Kannan, Synthesis and sintering of hydroxyapatite–zirconia composites, Mater. Sci. Eng. C 20 (2002) 187–193.
[5] V.V. Silva, F.S. Lameiras, R.Z. Domínguez, Microstructural and mechanical study of zirconia–hydroxyapatite (ZH) composite ceramics for biomedical applications, Comp. Sci. Technol. 61 (2001) 301–310.
[6] S. Nath, K. Biswas, K. Wang, R.K. Bordia, B. Basu, Sintering, phase stability, and properties of calcium phosphate-mullite composites, J. Am. Ceram. Soc. 93 (2010) 1639–1649.
[7] S. Nath, K. Biswas, B. Basu, Phase stability and microstructure development in hydroxyapatite–mullite system, Scr. Mater. 58 (2008) 1054–1057.
[8] S. Nath, A. Dey, A.K. Mukhopadhyay, B. Basu, Nanoindentation response of novel hydroxyapatite–mullite composites, Mater. Sci. Eng. A 513 (2009) 197–201.
[9] S. Nath, B. Basu, M. Mohanty, P.V. Mohanan, *In vivo* response of novel calcium phosphate–mullite composites: results upto 12 weeks of implantation, J. Biomed. Mater. Res. B: Appl. Biomater. 90B (2009) 547–557.
[10] S. Nath, S. Kalmodia, B. Basu, In vitro biocompatibility of novel calcium phosphate-mullite composites, J. Biomater. Appl. (2011).
[11] S. Nath, A.K. Dubey, B. Basu, Mechanical properties evaluation of novel calcium phosphate–mullite biocomposites, J. Biomater. Appl., in press.
[12] M. Tokita, Mechanism of spark plasma sintering and its application to ceramics, Nyn Seramikkasu 10 (1997) S43–53.
[13] I. Akin, M. Hotta, F.C. Sahin, O. Yucel, G. Goller, T. Goto, Microstructure and densification of ZrB_2–SiC composites prepared by spark plasma sintering, J. Eur. Ceram. Soc. 29 (11) (2009) 2379–2385.
[14] G. Peng, X. Li, M. Liang, Z. Liang, Q. Liu, W. Li, Spark plasma sintered high hardness α/β Si_3N_4 composites with $MgSiN_2$ as additives, Scr. Mater. 61 (4) (2009) 347–350.
[15] R. Mazumder, D. Chakravarty, D. Bhattacharya, A. Sen, Spark plasma sintering of $BiFeO_3$, Mater. Res. Bull. 44 (3) (2009) 555–559.
[16] R. Kumar, K.H. Prakash, P. Cheang, K.A. Khor, Microstructure and mechanical properties of spark plasma sintered zirconia–hydroxyapatite nano-composite powders, Acta Mater. 53 (2005) 2327–2335.
[17] S.F. Li, H. Izui, M. Okano, W.H. Zhang, T. Watanabe, Mechanical properties of ZrO_2 (Y_2O_3)–Al_2O_3 nanocomposites with addition of hydroxyapatite prepared by spark plasma sintering, Mater. Sci. Forum. 631–632 (2009) 413–423.
[18] S. Kalmodia, S. Goenka, T. Laha, D. Lahiri, B. Basu, K. Balani, Microstructure, mechanical properties, and *in vitro* biocompatibility of spark plasma sintered hydroxyapatite–aluminum oxide–carbon nanotube composite, Mater. Sci. Eng. C 30 (8) (2010) 1162–1169.
[19] W. Rathje, Zur kentnis de phosphate: I. uber hydroxyapatite, Bodenk Pflernah 12 (1939) 121–128.
[20] G.R. Anstis, P. Chantikul, B.R. Lawn, D.B. Marshall, A critical evaluation of indentation techniques for measuring fracture toughness, J. Am. Ceram. Soc. 64 (1983) 553–557.
[21] R.J. Sharma, S.R. Chaphalkar, A.D. Adsool, Evaluating antioxidant potential, cytotoxicity and intestinal absorption of flavonoids extracted from medicinal plants, Int. J. Biotechnol. Appl. 2 (1) (2010) 1–5.

[22] Z. Shen, E. Adolfsson, M. Nygren, L. Gao, H. Kawaoka, K. Niihara, Dense hydroxyapatite–zirconia ceramic composites with high strength for biological applications, Adv. Mater. 13 (2001) 214–216.
[23] W. Li, L. Gao, Fabrication of HAp–ZrO_2 (3Y) nano-composite by SPS, Biomaterials 24 (2003) 937–940.
[24] D. Kawagoe, Y. Koga, E.H. Ishida, N. Kotobuki, H. Ohgushi, K. Ioku, Preparation of transparent hydroxyapatite ceramics by spark plasma sintering and cell culture test, Phosphorous Res. Bull. 20 (2006) 119–128.
[25] I.S. Byun, S.K. Sarkar, M.A. Jyoti, Y.K. Min, H.S. Seo, B.T. Lee, H.Y. Song, Initial biocompatibility and enhanced osteoblast response of Si doping in a porous BCP bone graft substitute, J. Mater. Sci. Mater. Med. 21 (6) (2010) 1937–1947.
[26] K.A. Kim, W.K. Lee, K.H. Lee, Y. Lim, Auto proliferation and release of growth factors in silica-stimulated Rat2 Cells, Ann. Occup. Hyg. 46 (2002) 18–21.
[27] M. Absher, M. Mortara, Effect of silica on the proliferative behavior of human lung fibroblasts, *In Vitro* 16 (5) (1980) 371–376.